ELSEVIER

12 August 1999

PHYSICS LETTERS B

Physics Letters B 460 (1999) 474–483

Study of jet production in p–N interactions at $\sqrt{s} \approx 500$ GeV in EAS multicore events

EAS–TOP Collaboration

M. Aglietta [a,b], B. Alessandro [b], P. Antonioli [c], F. Arneodo [d], L. Bergamasco [b,e], M. Bertaina [b,e], C. Castagnoli [a,b], A. Castellina [a,b], A. Chiavassa [b,e], G. Cini Castagnoli [b,e], B. D'Ettore Piazzoli [f], G. Di Sciascio [f], W. Fulgione [a,b], P. Galeotti [b,e], P.L. Ghia [a,b], M. Iacovacci [f], G. Mannocchi [a,b], C. Morello [a,b], G. Navarra [b,e], L. Riccati [b], O. Saavedra [b,e], G.C. Trinchero [a,b], P. Vallania [a,b], S. Vernetto [a,b], C. Vigorito [a,b,1]

[a] *Istituto di Cosmo-Geofisica del CNR, Torino, Italy*
[b] *Istituto Nazionale di Fisica Nucleare, Sezione di Torino, Italy*
[c] *Istituto Nazionale di Fisica Nucleare, Sezione di Bologna, Italy*
[d] *Istituto Nazionale di Fisica Nucleare, Laboratori Nazionali del Gran Sasso, Assergi, L'Aquila, Italy*
[e] *Dipartimento di Fisica Generale dell'Università di Torino, Italy*
[f] *Dipartimento di Scienze Fisiche dell' Università di Napoli and INFN, Sezione di Napoli, Italy*

Received 25 March 1999
Editor: K. Winter

Abstract

The cross section for large p_t jet production for transverse momentum $10 \le p_t \le 20$ GeV/c and rapidity $1.6 \le \eta \le 2.6$ in p–N (p–'air') interactions is studied from the analysis of multicore Extensive Air Showers recorded in the EAS–TOP calorimeter. The projectiles are the leading particles interacting at atmospheric depths between 250 and 480 cm^{-2}, the CMS energy of interaction being $\sqrt{s} \approx 500$ GeV. The slope of the p_t distribution agrees with the expected one from the p–$\bar{p}$ collider data at the same CMS energy. The measured jet production cross section in p–N interactions with respect to p–$\bar{p}$ interactions is $(d\sigma/dp_t)^{\mathrm{jet}}_{pN} = (d\sigma/dp_t)^{\mathrm{jet}}_{p\bar{p}} \cdot A^{\alpha}$ with $\alpha = 1.56 \pm 0.07$ for $A = 14.7$ (average mass number of 'air' nuclei). Such value is compatible within the experimental uncertainties with the one obtained in p–nucleus accelerator measurements at $\sqrt{s} \simeq 30$ GeV in the same range of transverse momentum and rapidity. No indication of increase of α with energy, i.e. of the entity of the 'Cronin effect', is found.

PACS: 13.87.Ce; 13.85.Tp; 96.40.Pq
Keywords: Large transverse momentum; Jet; Proton-nucleus interactions; EAS; EAS multicores

[1] Corresponding author: Dr. C. Vigorito, postal address: Dipartimento di Fisica Generale, via P. Giuria 1, 10125 Torino, Italy. Tel. +39-011-6707498, Fax +39-011-6707493, E-mail: vigorito@to.infn.it

0370-2693/99/$ - see front matter
PII: S0370-2693(99)00782-0

1. Introduction

Jet production has been studied at colliders in p–$\bar{p}$ interactions up to $\sqrt{s} \simeq 630$ GeV [1,2] and $\sqrt{s} \simeq 1.8$ TeV [3], and in p–nucleus interactions in fixed target experiments up to $\sqrt{s} \simeq 30$ GeV [4,5].

In Extensive Air Shower (EAS) experiments, multicore events (i.e. events with multiple structure in the e.m. component near the axis) have been observed since '60's [6–10] and their interpretation as due to jet production has lead to first information on production cross sections [10]. The consistency of the observations in different cosmic rays experiments has been recently discussed in [11,12]. In the case of multicore EAS, jets are essentially produced by the leading particle interactions with 'air' target nuclei at intermediate altitudes in the atmosphere ($z \approx 6$–12 km above sea level) at typical energies $\sqrt{s} \approx (300$–$1000)$ GeV. Such experiments allow thus the extension of p–nucleus accelerator data and the direct comparison with p–$\bar{p}$ collider measurements.

In the present paper we report the measurement of the jet production cross section at $\sqrt{s} \approx 500$ GeV for $10 \leq p_t \leq 20$ GeV/c and pseudo-rapidity $1.6 \leq \eta \leq 2.6$. The result leads to the measurement of α $((d\sigma/dp_t)^{\rm jet}_{pN} = (d\sigma/dp_t)^{\rm jet}_{p\bar{p}} \cdot A^{\alpha})$ for $A = 14.7$ (average mass number of the 'air' target nuclei) which is compared with existing p–nucleus data at fixed target experiments.

From the point of view of cosmic rays physics, the effect can be relevant for experiments exploiting the high energy component in the core region to draw informations on the cosmic ray primary composition.

2. The experiment

The measurement is performed at the EAS–TOP array [13,14] (Campo Imperatore, 2005 m a.s.l., National Gran Sasso Laboratories). EAS core investigations are performed by means of its calorimeter [15]. EAS data, i.e. shower sizes (total number of charged particles, N_e) and arrival directions, are obtained from the electromagnetic detector [16].

The EAS–TOP calorimeter is a parallelepiped of dimensions $12 \times 12 \times 3$ m^3 and consists of 9 identical planes. Each active plane is made of two layers of *streamer* tubes for muon tracking and a layer of *quasi proportional* tubes (3×3 cm^2 section, 12 m length) for hadron calorimetry, separated by 13 cm thick iron absorbers, for a total depth $x = 818$ g cm^{-2}, i.e. $x_\lambda \simeq 6.2$ nuclear mean free paths. The read-out of the quasi proportional tubes is performed by induction through a matrix of 840 pads (40×38 cm^2) placed on top of each level for a total area of 128 m^2. The active layers of the upper plane (9th) are unshielded and operate as a fine grain detector of the electromagnetic component of EAS cores. The ADC outputs are converted to the equivalent particle numbers by using single particle responses obtained in ad hoc calibration runs and linearity data.

A model of the response of the *quasi proportional* chambers to large particle densities has been developed and checked through on site measurements and a test at CERN facilities with a 50 GeV e^+ beam. Such model has been included into a simulation of hadronic cascades initiated in the atmosphere (CORSIKA-HDPM code, [17]) and propagated through the calorimeter (GEANT code, [18]) to study their absorption properties and the energy determination.

The beam test allowed to check the measured response fluctuation of individual pads as a function of the recorded particle number N:

$$\left(\frac{\sigma}{N}\right)^2 = a^2 + \frac{b^2}{N} \qquad (1)$$

with $a = 0.16$ and $b = 2.15$.

Eight (80×80 cm^2) scintillator counters, identical to the ones of the EAS–TOP e.m. detector are located above the 9th plane: 4 internal (P_i) are placed at about 3 m from the calorimeter center and 4 external (M_i) outside the module structure at its corners. They are used to select contained EAS cores.

The detector layout is shown in Fig. 1.

The e.m. detector is made of 35 scintillator modules, 10 m^2 each, distributed over an area $A_{\rm eff} \approx 10^5$ m^2, separated by $d \approx 20$ m in the region near the calorimeter and $d \approx 80$ m in the outside area. From the sample of the particle densities at the different positions and the time of flight between the detec-

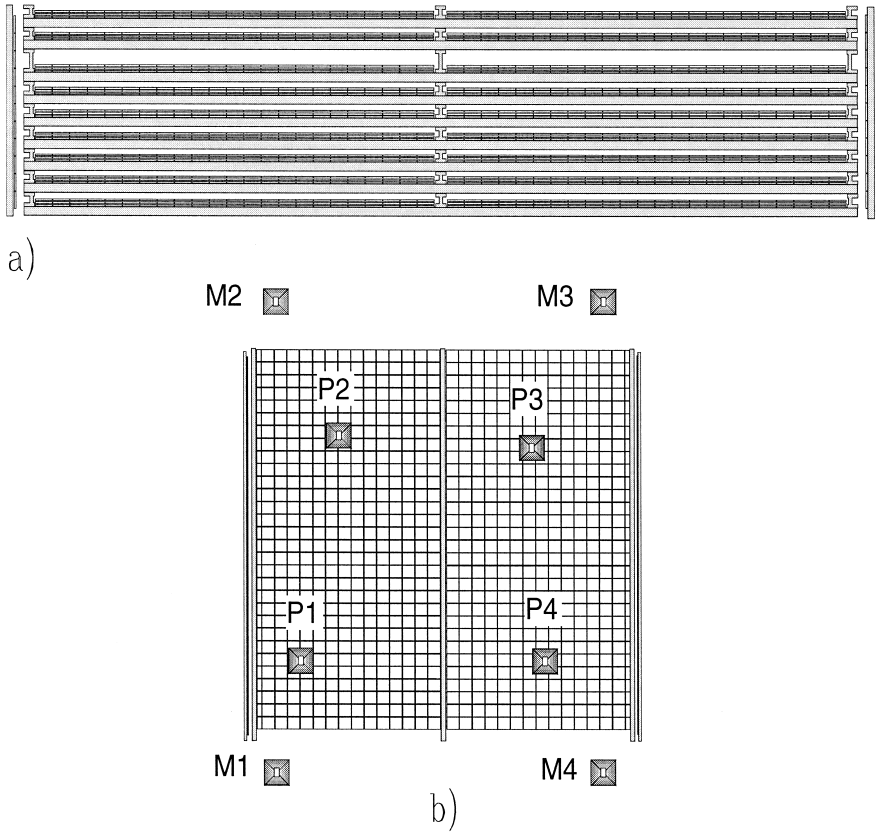

Fig. 1. Layout of the EAS–TOP calorimeter: (a) frame, iron absorbers, layer chamber structure and vertical walls; (b) 9th plane, top view, including the M_i and P_i scintillators.

tors, the core location, the slope of the lateral distribution function (l.d.f.), the shower size (N_e) and the EAS arrival direction (θ, ϕ) are obtained (see details in the following).

3. Data selection

3.1. EAS analysis

In the present analysis only Extensive Air Showers which triggered both the electromagnetic and hadronic detectors have been considered.

The data acquisition of the whole e.m. array is enabled by any fourfold coincidence ($\Delta t = 350$ ns, rate ≈ 20 Hz) of 4 nearby modules (threshold 0.3 m.i.p. per module).

The full read-out of the hadron detector is triggered by the fourfold coincidence of the P_i scintillators (1 m.i.p. threshold) and the condition of at least 200 particles on the uppermost proportional layer of the calorimeter (rate ≈ 1.2 Hz).

Data recorded by the two detectors are time correlated off-line ($|\Delta t| < 10\ \mu$s).

EAS with core hitting the calorimeter are first selected with scintillators (M_i, P_i, with recorded numbers of particles N^{M_i} and N^{P_i}) using the following condition:

$$R = \frac{\sum_{i=1}^{4} N^{M_i}}{\sum_{i=1}^{4} N^{P_i}} \leq 1 \qquad (2)$$

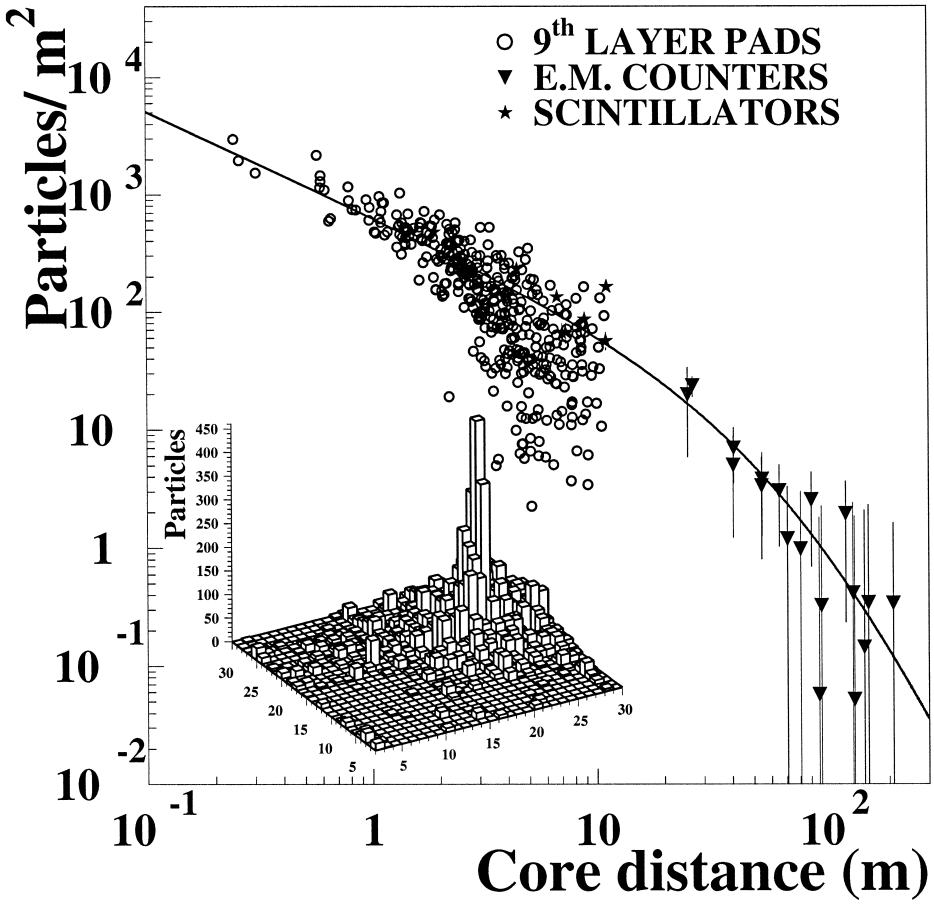

Fig. 2. A single core EAS: the reconstructed lateral distribution function and the core region as observed by the upper unshielded layer of the calorimeter are shown.

The shower size and core location are reconstructed through a fit to the NKG theoretical particle distribution [2] of the recorded particle densities in the upper level (with pad recorded particle numbers $N_{i,j}$), the M_i and P_i scintillators and the e.m. counters of the array. Events with core located inside a fiducial area of 8×8 m^2 centered on the calorimeter and with zenith angle $\theta \leq 35^0$ are selected for further analysis.

For shower size $N_e \geq 10^5$ the reconstruction efficiency is $\epsilon \geq 95\%$, the resolution $\frac{\Delta N_e}{N_e} \leq 15\%$ and the accuracy on the arrival direction measurement $\sigma_\theta \approx 0.5°$; in 70% of events the fitted core position is found at distance $d \leq 70$ cm from the pad with maximum recorded particle density. It must be pointed out that, even in presence of substructures, the fitted main core location is usually positioned in the vicinity of the maximum recorded particle density; i. e. the presence of the substructure does not displace the core location which is determined by a very large number of symmetrical measurements. A typical single core event is shown in Fig. 2 together with the reconstructed l.d.f.

The present analysis includes data recorded between December 1995 and February 1998: 5322 events in the size range $10^{5.26} \leq N_e \leq 10^{5.60}$, i.e.

[2] $\rho(r) = c(s)\frac{Ne}{(r_0)^2}(1+\frac{r}{r_0})^{s-4.5}(\frac{r}{r_0})^{s-2}$: Nishimura-Kamata-Greisen theoretical lateral distribution function for electrons for shower size N_e and slope s ($r_0 = 100$ m) [19].

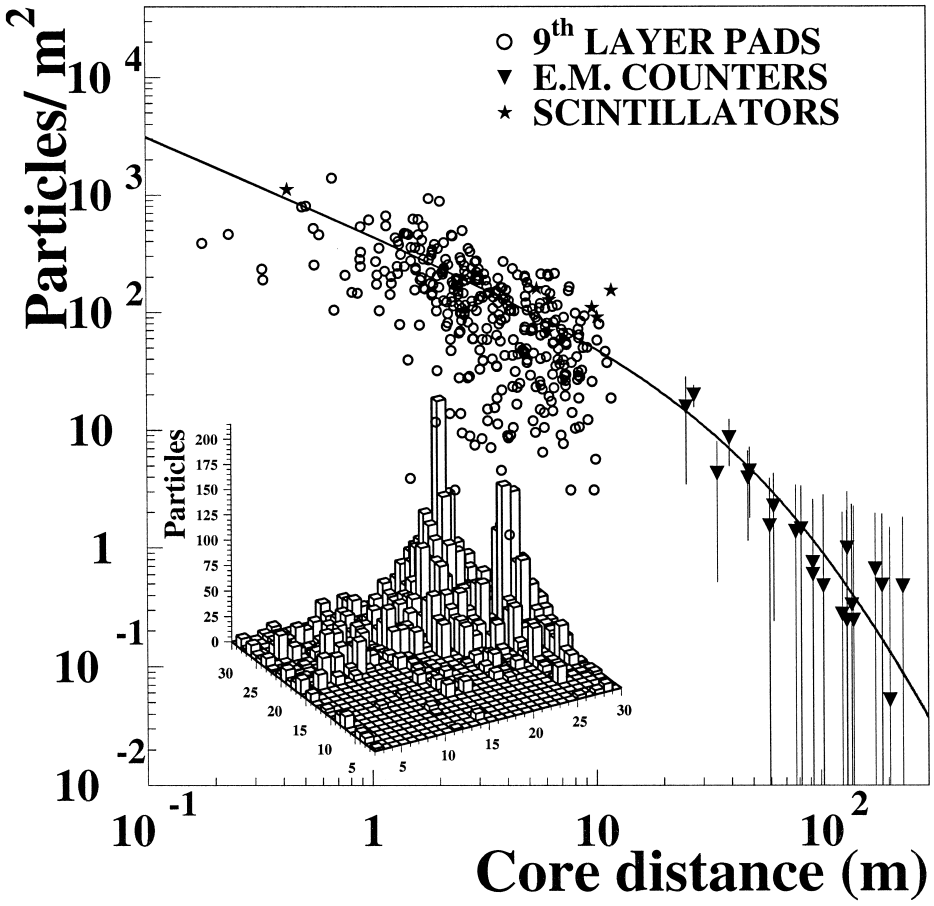

Fig. 3. A multicore EAS: the reconstructed lateral distribution function of the main shower and the central region are shown.

primary energy [3] between 500 and 1000 TeV for primary protons.

3.2. Multicore events selection

Multicore events are selected from the analysis of the e.m. component recorded on the uppermost layer of the calorimeter. First, each event is fully reconstructed, as previously described, to get shower size (N_e), core location, arrival direction and slope (s) of lateral distribution function (see Fig. 3). These data provide the expected average number of particles $\overline{N}_{i,j}$ and the corresponding fluctuation (following expression (1): $\sigma_{i,j}(\overline{N}_{i,j})$) on each (i,j) pad of the unshielded layer. Then by applying a cluster algorithm to the matrix of the quantities:

$$S_{i,j} = \frac{N'_{i,j}}{\sigma_{i,j}\left(\overline{N}_{i,j}\right)} \quad \left(N'_{i,j} = N_{i,j} - \overline{N}_{i,j}\right) \tag{3}$$

subcore structures in the e.m. component are extracted. For each (i,j) point of the matrix having $S_{i,j} \geq 5$, the quantity $Q = \Sigma_{(i,j)} S_{i,j}$ is calculated by summing over all the pads included inside a radius ranging from 0.4 to 2.0 m (0.4 m step). The cluster with maximum Q value is chosen and its position is defined as the barycenter of its $N'_{i,j}$ quantities. The distance r of the structure from the main core is thus

[3] The shower size (N_e) to energy (E_0) conversion used is: $E_0(\mathrm{TeV}) = \alpha \cdot N_e^{\beta}$ with $\alpha = 0.0084$ and $\beta = 0.903$, obtained by means of a simulation (CORSIKA-HDPM [17]) for primary protons [20].

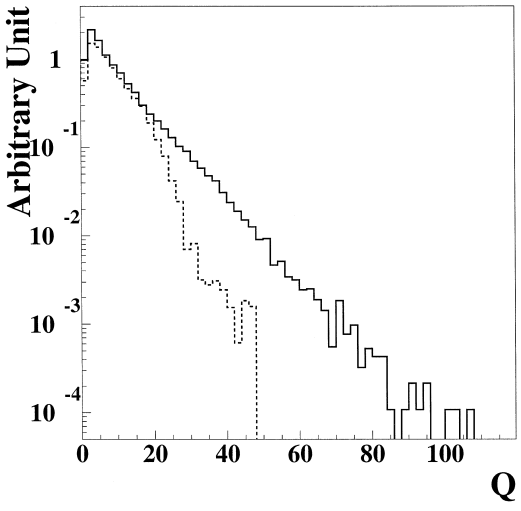

Fig. 4. Distribution of Q values (see text) for selected clusters in real data (full line) and in simulated single core showers including experimental fluctuations (dashed line).

obtained. The accuracy on the subcore position determination is $\Delta r \approx 40$ cm. A cut on distance, $r \geq 1.5$ m, has been applied to cut off possible contributions to the substructure due to fluctuations of the main core pads. The typical number of pads involved in the subcore is $n_p \approx 20$.

The contribution of false clusters, due to the fluctuations of the pad responses in single core events and recognized by the algorithm, has been evaluated by means of a simulation. The NKG l.d.f. is used, since it represents a good fit to standard showers also in the vicinity of the core; fluctuations following expression (1) are included. The experimental and simulated distributions of the quantity Q for each detected structure are shown in Fig. 4. The two distributions coincide for $Q < 20$, dominated by fluctuations effects, while a cut $Q \geq 20$ selects physical events.

3.3. Energy and production height determinations

For the energy and production height determinations of each subcore, the quantities:

$$P_9 = \sum_{(i,j)}^{20} N'_{i,j} \qquad (4)$$

at the uppermost level (i.e. the electromagnetic content) and

$$S_8 = \sum_{k=1}^{8} \sum_{(i,j)}^{20} N'_{i,j,k} \qquad (5)$$

($N'_{i,j}$ defined for each layer k as in expression (3)) integrated over the 8 internal layers (i.e. the hadronic and high energy e.m. contents), are used. The sum involves the 20 most significant pads inside the structure within 1 m from the subcore position on the uppermost plane and, for internal ones, from its projected position following the EAS direction. For internal layers $\bar{N}_{i,j}$ is obtained from the pads at the same distance r from the main core, not belonging to the subcore structure.

The resulting scatter plot P_9–S_8 for physical events is shown in Fig. 5. The same plot is shown in Fig. 6 for simulated primary proton showers of different energies initiated at the top and at different atmospheric depths ranging between 6000 and 11000 m a.s.l.. From the comparison of Figs. 5 and 6 it results that the pattern of the selected subcore structures falls in the region characterized by intermediate starting levels in the atmosphere. Top events are excluded since they should have a much higher hadronic content for the same electromagnetic size

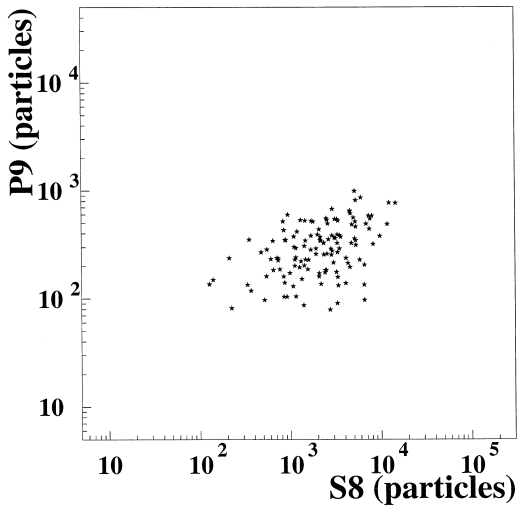

Fig. 5. Scatter plot of cluster patterns (P_9,S_8) of the detected secondary structures in 130 multicore EAS.

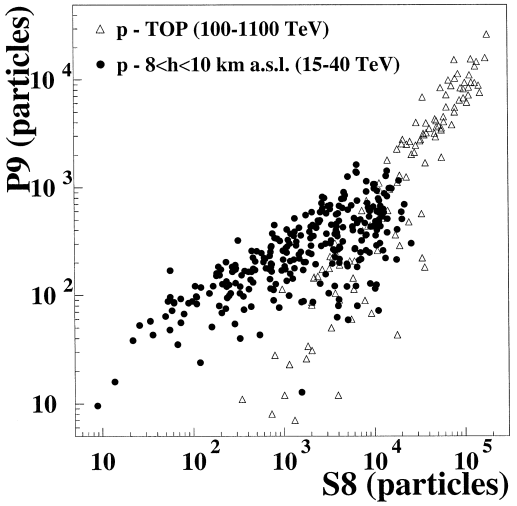

Fig. 6. Scatter plot of cluster patterns (P_9,S_8), showing the difference between showers initiated at the top and at lower atmospheric levels.

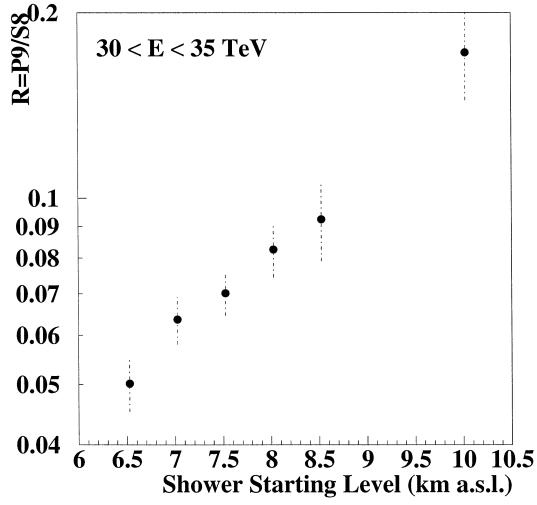

Fig. 7. Behaviour of ratio $R = P_9 / S_8$ (see text) with the production height in the energy range $30 \le E_s \le 35$ TeV.

(and it must be pointed out that the patterns of the P_9–S_8 parameters for the main shower cores agree with the expectations for showers initiated at the top). This proves that the subcores are produced by interactions in the cascade development in the atmosphere occurring at altitudes $\bar{z} \approx 9000$ m above sea level.

The subcore primary energy is assigned by using the P_9 measurement:

$$E_s(\mathrm{TeV}) = a \cdot P_9^b \qquad (6)$$

with $a = 0.69 \pm 0.05$ and $b = 0.64 \pm 0.01$, obtained through the quoted simulation assuming the shower at its maximum development.

The estimated error on energy measurement (also obtained from the simulation) is $\Delta E_s/E_s = 42\%$.

Moreover the ratio $R = P_9/S_8$ is sensitive to the starting point in the atmosphere and, to less extent, to the subcore energy, as shown in Fig. 7. The production height is obtained from the experimental values of R and E_s(TeV) (with uncertainty $\Delta z/z = 27\%$) using the expression:

$$z(m) = C_1 \cdot \log(E_s) + C_2 \cdot \log(R) + C_3 \qquad (7)$$

where $C_1 = 9.1 \pm 0.9$, $C_2 = 1850 \pm 40$ and $C_3 = 12840 \pm 280$ m. Events with production height $6000 \le z \le 11000$ m a.s.l., i.e. $250 \le x \le 480$ gcm^{-2} for vertical incidence, are considered. In Fig. 8 the distributions of energy E_s, production height z and distance r from shower axis of the detected subcores are shown.

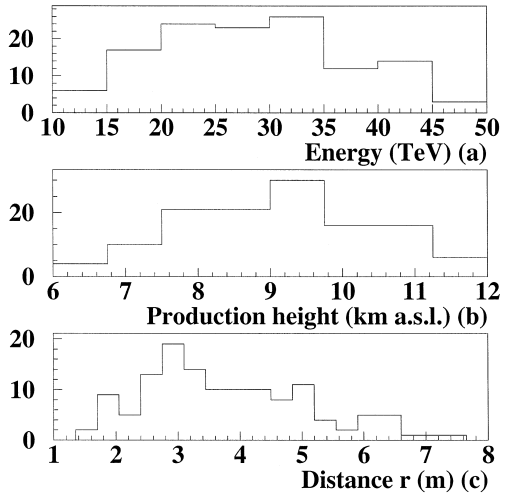

Fig. 8. Distributions of the reconstructed energies (a), production heights (b), distances from main core (c) of the detected subcores.

4. The jet analysis

For energy determination, the jet fragmentation [2] has been taken into account by means of a simulation of jets produced at the reconstructed altitudes: a fraction $\epsilon_E \simeq 86\%$ of the jet energy is expected to be inside the detected subcore structure. Such efficiency has been introduced in the final energy evaluation.

The subcore detection efficiency ($\epsilon_d(N_e, E_s, r)$, shown in Fig. 9) has been calculated by simulating showers of energy E_s, at distance r from the main core, averaging over the distributions of production heights and shower sizes for $10^{5.26} \leq N_e \leq 10^{5.60}$. A cut on distance $r \geq 3$ m and subcore energy $E_s \geq 15$ TeV is performed in order to select a region with reconstruction efficiency $\epsilon_d(N_e, E_s, r) \geq 5\%$.

In the quoted size range, 64 subcores have been selected. The transverse momentum for each of them has been obtained using expression:

$$p_t^{\text{meas}} = \frac{E_s \cdot r}{\epsilon_E \cdot h} \tag{8}$$

where $h = z - 2005$ m is the production height above the observation level. The obtained p_t^{meas} values are in the range 10–30 GeV/c. From the uncertainties in the measurements of E_s, r and h, as obtained from the quoted simulation, we get as error in p_t^{meas}:

$$\Delta p_t^{\text{meas}} / p_t^{\text{meas}} \approx 50\% \tag{9}$$

At intermediate interaction levels (see Fig. 8b) the projectiles contributing to high energy events can be associated, as first suggested in [8,10], to the leading particles inside the showers. In fact, the leading particles dominate (10:1) over the secondaries in 1000 TeV showers for energies large enough to produce cascades with the energy distribution of Fig. 8a (i.e. $E_s > 15$ TeV). The leading particle spectrum has been derived from the cosmic ray primary spectrum by scaling the corresponding energy to the mean production depth of subcores, with the attenuation length $\Lambda = 100$ gcm^{-2}:

$$E_{\text{l.p.}} = E_0 \cdot e^{-\frac{X}{\Lambda}} \tag{10}$$

At the mean production height $\bar{z} \approx 9000$ m a.s.l., i.e. atmospheric depth $X \approx 270$ gcm^{-2} (see Fig. 8b) the leading particle energy, averaged over the primary spectrum in the range 500–1000 TeV here analysed, is $E_{\text{l.p.}} \approx 125$ TeV corresponding to $\sqrt{s} \approx 500$ GeV for p–p interactions. (Such results are in agreement with the expectation obtained from full simulations based on the CORSIKA code).

The uncertainty on the attenuation length Λ:

$$\Delta\Lambda / \Lambda \approx 10\% \tag{11}$$

reflects in an uncertainty on $E_{\text{l.p.}}$:

$$\Delta E_{\text{l.p.}} / E_{\text{l.p.}} \approx 26\% \tag{12}$$

The scanned rapidity interval has been obtained by means of a geometrical simulation of the detector acceptance for subcore detection as a function of the production height h and distance from the main shower $r \geq 3$ m. The resulting efficiency, for detecting pseudo-rapidity η, is:

$$\epsilon_R(\eta) = a + b \cdot \eta \tag{13}$$

where $a = -2.74 \pm 0.13$ and $b = 0.401 \pm 0.016$.

The accepted region of pseudo-rapidity $7.8 \leq \eta \leq 8.8$, i.e. $1.6 \leq \eta_{\text{c.m.}} \leq 2.6$ in the CMS of the interaction, corresponds to values of $\epsilon_R(\eta)$ exceeding 40%.

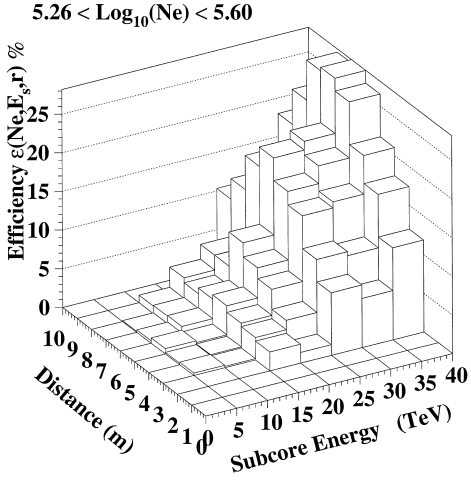

Fig. 9. Efficiency of subcore detection as a function of energy (E_s) and distance from main core axis (r) for a given shower size.

5. Results

The rate of large p_t^{meas} events per shower is obtained by applying to each of the n_{bin} events of

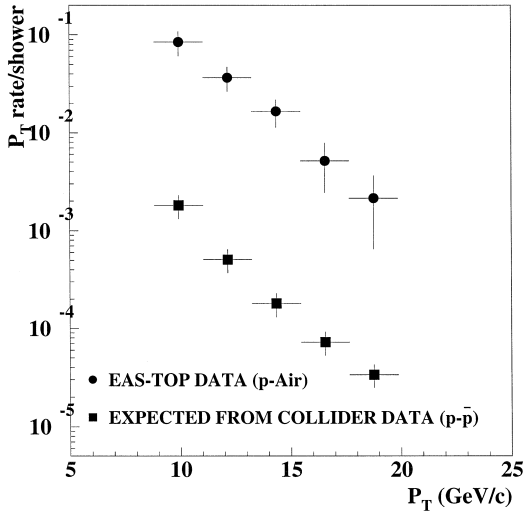

Fig. 10. Measured p_t rate in multicore EAS compared with the expected one from $p-\bar{p}$ collider cross section data.

bin $(p_t^{\mathrm{meas}}, p_t^{\mathrm{meas}} + \Delta p_t^{\mathrm{meas}})$ the detection efficiency $\epsilon_d^i(N_e, E_s, r)$ and the geometrical acceptance $\epsilon_R^i(\eta)$:

$$f(p_t^{\mathrm{meas}}) = \frac{1}{N_{EAS}} \sum_{i=1}^{n_{\mathrm{bin}}} \frac{1}{\epsilon_d^i \cdot \epsilon_R^i} \tag{14}$$

The reported uncertainty in the measurement of transverse momentum (9), together with the steepness of the slope of the p_t^{meas} distribution ($f(p_t^{\mathrm{meas}}) \propto (p_t^{\mathrm{meas}})^{-\delta}$) introduces a systematic overestimate of the transverse momentum, so that

$$p_t^{\mathrm{meas}} = (1.35 \pm 0.05) \cdot p_t \tag{15}$$

(for $\delta = 6.04 \pm 0.56$ obtained from the fit to the experimental data, see Fig. 10). The individual p_t^{meas} values have therefore been shifted by factor (15).

The obtained p_t distribution is shown in Fig. 10.

In the same figure, the p_t rate per shower, calculated from the collider cross section data $d\sigma/dp_t$ [4] in the same rapidity interval, assuming as target nuclei single protons, is shown. The values have been calculated by means of the following integration:

$$N_{p_t}^{p_t+\Delta p_t} = \int_{p_t}^{p_t+\Delta p_t} \left(\frac{dN}{dp_t}\right)_{p\bar{p}} dp_t = \int_{p_t}^{p_t+\Delta p_t} dp_t \int_{250}^{480} dx \left\langle \frac{d\sigma}{dp_t} \right\rangle_{\theta, E_0} \frac{N_A}{A} \tag{16}$$

with $N_A =$ Avogadro number, $A = 14.7$ (average mass number of 'air' nuclei target), $x =$ atmospheric depth [gcm^{-2}] and $\langle \frac{d\sigma}{dp_t} \rangle_{\theta, E_0}$:

$$\left\langle \frac{d\sigma}{dp_t} \right\rangle_{\theta, E_0} = \frac{\int_0^{0.6} \cos(\theta)\sin(\theta)\, d\theta \int_{500}^{1000} E_0^{-\gamma}\, dE_0 \cdot \left(\frac{d\sigma(\sqrt{s})}{dp_t}\right)_{p\bar{p}}}{\int_0^{0.6} \cos(\theta)\sin(\theta)\, d\theta \int_{500}^{1000} E_0^{-\gamma}\, dE_0} \tag{17}$$

with $\theta =$ arrival zenith angle of the shower [rad], $E_0 =$ cosmic ray primary energy [TeV] and $\sqrt{s} = \sqrt{s}(E_0, x, \theta)$ following expression (10).

Also included in Fig. 10 are the statistical and systematic errors, i.e.:

- concerning the calculation, the uncertainties of the experimental collider data and of Λ (by introducing uncertainty (12) in expression (16));
- concerning the experimental data, the main systematic error ($\approx 18\%$) which is due to the uncertainty in correction (15).

The slopes of the two distributions, $f(p_t) \propto p_t^{-\delta}$, with $\delta = 6.16 \pm 0.09$ for the calculated one for $p-\bar{p}$ interactions, and $\delta = 6.04 \pm 0.56$ for the experimental one for $p-N$ interactions, are in agreement inside the experimental errors. This shows that the p_t dependencies of $p-\bar{p}$ and $p-N$ jet production cross sections ($d\sigma/dp_t$) are compatible.

The gap in the absolute rates reflects the difference between $p-\bar{p}$ and $p-N$ cross sections.

The ratio $R = (d\sigma/dp_t)_{pN}^{\mathrm{jet}} / (d\sigma/dp_t)_{p\bar{p}}^{\mathrm{jet}}$ is constant versus the transverse momentum and is on average: $\bar{R} = 60.4 \pm 12.9$.

By representing such gap following the usual expression:

$$(d\sigma/dp_t)_{pN}^{\mathrm{jet}} = (d\sigma/dp_t)_{p\bar{p}}^{\mathrm{jet}} \cdot A^{\alpha}$$

[4] The invariant cross section used is: $\frac{Ed^3\sigma}{dp^3} = p_t^{-n} f(x_t)$ with $f(x_t) = C\frac{(1-x_t)^m}{x_t^2}$, $n = 4.74 \pm 0.06$, $m = 6.54 \pm 0.15$, $C = (8.3 \pm 0.4) \cdot 10^{-29}$ cm^2 GeV^{n-2} and $x_t = 2p_t/\sqrt{s}$ [1].

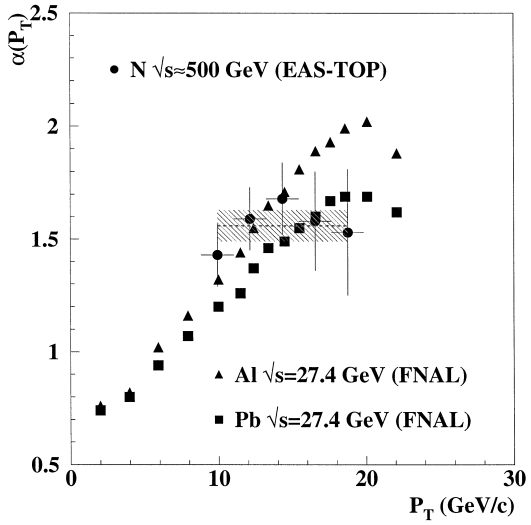

Fig. 11. Present measurement of the exponent index α ($(d\sigma/dp_t)^{\rm jet}_{pN} = (d\sigma/dp_t)^{\rm jet}_{p\bar{p}} \cdot A^{\alpha}$) compared with the existing data at fixed target experiments. The dashed box indicates, in the range $10 \le p_t \le 20$ GeV/c, the mean value of α with its uncertainty.

with $A = 14.7$ (mean atomic number of 'air' nuclei target) the value:

$\alpha = 1.56 \pm 0.07$

is obtained.

Such value is compared with existing fixed target accelerator data (Al and Pb targets [21–23]) in Fig. 11. The measured values of α agree in the same range of transverse momentum and pseudo-rapidity, showing that no change in the $(d\sigma/dp_t)^{\rm jet}_{pN}/(d\sigma/dp_t)^{\rm jet}_{p\bar{p}}$ ratio of jet production cross sections occurs between $\sqrt{s} \simeq 30$ GeV and $\sqrt{s} \simeq 500$ GeV.

6. Conclusions

The $(d\sigma/dp_t)^{\rm jet}_{pN}$ cross section for high p_t jet production at primary energy $\sqrt{s} \approx 500$ GeV, $10 \le p_t \le 20$ GeV/c and rapidity $1.6 \le \eta \le 2.6$ is measured by means of multicore Extensive Air Showers recorded by the EAS–TOP detector in p–air interactions ($A = 14.7$).

The slopes of the p_t distributions of p–$\bar{p}$ and p–N jet production cross sections are compatible at 10% level.

The obtained value of the exponent index α in the expression $(d\sigma/dp_t)^{\rm jet}_{pN} = (d\sigma/dp_t)^{\rm jet}_{p\bar{p}} \cdot A^{\alpha}$ is $\alpha = 1.56 \pm 0.07$. Such value agrees with the one obtained in fixed target accelerator experiments at $\sqrt{s} \approx 30$ GeV.

It is shown that no change of the value of α occurs between $\sqrt{s} \approx 30$ GeV and $\sqrt{s} \approx 500$ GeV.

Acknowledgements

The continuous cooperation of the Director and of the Staff of the Gran Sasso National Laboratories, as well as the technical assistance of C. Barattia, R. Bertoni, A. Giuliano, G. Giuliani and G. Pirali are gratefully acknowledged.

References

[1] J.A. Appel et al., Phys. Lett. B 160 (1985) 349.
[2] L. Di Lella, Ann. Rev. Nucl. Part. Sci. 35 (1985) 107.
[3] F. Abe et al., Phys. Rev. Lett. 65 (1990) 968.
[4] J.W. Cronin et al., Phys. Rev. D 11 (1975) 3105.
[5] S. Fredriksson et al., Phys. Rep. 144 (1987) 187.
[6] W.E. Hazen, R.E. Heineman, Phys. Rev. 90 (1953) 496.
[7] T. Matano et al., Canad. J. Phys. 46 (1968) S56.
[8] A.M. Bakich et al., Canad. J. Phys. 46 (1968) S30.
[9] G. Bosia et al., Il Nuovo Cimento C 3 (1980) 215.
[10] A.E. Chudakov et al., Proc. XVII ICRC 6 (Paris) (1981) 183.
[11] M. Aglietta et al., Nuovo Cimento C 18 (1995) 663.
[12] A.S. Lidvansky, Proc. XXV ICRC 6 (Durban) (1997) 169.
[13] M. Aglietta et al., Nucl. Instr. and Meth. A 277 (1988) 23.
[14] M. Aglietta et al., Nucl. Phys. B 54 (1997) 263.
[15] EAS–STOP Collaboration, Nucl. Instr. and Meth. A 420 (1999) 117.
[16] M. Aglietta et al., Nucl. Instr. and Meth. A 336 (1993) 310.
[17] J.N. Capdevielle et al., The Karlsruhe EAS simulation code CORSIKA, KFK Report 4998, 1992.
[18] Application Software Group and Network Division, GEANT: Detector description and Simulation tool 3.21, CERN, W5013, 1994.
[19] K. Kamata et al., Suppl. Progr. Theor. Phys. 6 (1958) 93.
[20] EAS–TOP Collaboration, Astroparticle Phys. 10 (1999) 1.
[21] B. Brown et al., Phys. Rev. Lett. 50 (1983) 11.
[22] J. Rice et al., Nucl. Phys. A 418 (1984) 315.
[23] H. Miettinen et al., Phys. Lett. B 207 (1988) 22.